



Integration-based extraction and visualization of jet stream cores

Lukas Bösigler¹, Michael Sprenger², Maxi Boettcher², Hanna Joos², and Tobias Günther³

¹Department of Computer Science, ETH Zurich, Zurich, Switzerland

²Institute for Atmospheric and Climate Science, ETH Zurich, Zurich, Switzerland

³Department of Computer Science, FAU Erlangen-Nürnberg, Erlangen, Germany

Correspondence: Tobias Günther (tobias.guenther@fau.de)

Received: 14 July 2021 – Discussion started: 27 August 2021

Revised: 23 November 2021 – Accepted: 20 December 2021 – Published: 4 February 2022

Abstract. Jet streams are fast three-dimensional coherent air flows that interact with other atmospheric structures such as warm conveyor belts (WCBs) and the tropopause. Individually, these structures have a significant impact on the midlatitude weather evolution, and the impact of their interaction is still a subject of research in the atmospheric sciences. A first step towards a deeper understanding of the meteorological processes is to extract the geometry of jet streams, for which we develop an integration-based feature extraction algorithm. Thus, rather than characterizing jet core line purely as extremal line structure of wind magnitude, our core-line definition includes a regularization to favor jet core lines that align with the wind vector field. Based on the line geometry, proximity-based filtering can automatically detect potential interactions between WCBs and jets, and results of an automatic detection of split and merge events of jets can be visualized in relation to the tropopause. Taking ERA5 reanalysis data as input, we first extract jet stream core lines using an integration-based predictor–corrector approach that admits momentarily weak air streams. Using WCB trajectories and the tropopause geometry as context, we visualize individual cases, showing how WCBs influence the acceleration and displacement of jet streams, and how the tropopause behaves near split and merge locations of jets. Multiple geographical projections, slicing, as well as direct and indirect volume rendering further support the interactive analysis. Using our tool, we obtained a new perspective on the three-dimensional jet movement, which can stimulate follow-up research.

1 Introduction

Meteorologists face the challenge of making sense out of highly complex atmospheric data, which are large, three-dimensional, and time dependent, and contain multiple fields. These data are traditionally examined in 2-D (Rautenhaus et al., 2018), with more modern approaches transitioning towards 3-D (Li et al., 2019; Rautenhaus et al., 2015b). This is because the atmospheric circulation contains and is governed by numerous three-dimensional flow features and processes that significantly impact the weather (Nielsen-Gammon, 2001; Harnik et al., 2016). For example, near the tropopause, the boundary between the troposphere and the stratosphere, we can find fast coherent air streams called jet streams (Koch et al., 2006; Schiemann et al., 2009). The wind speed of jet streams often exceeds 50 m s^{-1} at their core, as they meander from west to east around the planet (Ahrens and Henson, 2018). Jet streams can interact with the tropopause as well as with outflows of warm conveyor belts (WCBs), which are strongly slantwise and coherently ascending air streams within extratropical cyclones that diverge at the tropopause (Madonna et al., 2014). Both jets and WCBs are well known to play a major role in midlatitude weather evolution and predictability (Harnik et al., 2016; Manney et al., 2014; Manney and Hegglin, 2018). However, how much they influence each other and which physical processes are involved in this interaction has not yet been fully explored in the atmospheric sciences.

In this paper, we aim for an explicit extraction of jet stream core-line geometry, which enables automatic detection of proximity to WCBs and allows for the automatic extraction of split and merge events. We visually investigate the shape of the three-dimensional tropopause near the split and merge

events by visualizing the structures in 3-D. This requires a robust extraction algorithm emitting long jet stream core lines that are temporally stable and long enough to find split and merge locations. To this end, we extend the recent work of Kern et al. (2017), who developed a local jet core extraction algorithm, which may result in fragmented core-line segments when the velocity magnitude temporally falls below a required threshold. Thus, instead, we extract the jet stream as an instantaneous flow feature from the atmospheric data using a predictor–corrector approach (Banks and Singer, 1994) that follows the flow and corrects the trajectories towards the ridge lines of the wind magnitude field. This way, we can balance between two constraints: maximizing the wind speed and aligning with the flow direction. The latter serves as regularization to prevent unnaturally bent ridge lines caused by a low vertical resolution. Thereby, jet stream core lines are allowed to fall below the magnitude threshold for a user-defined period of time. To display context and to locate possible interactions with other atmospheric structures, we extract the tropopause based on its dynamical definition and select WCBs as path lines fulfilling a necessary ascent criterion in the neighborhood of extratropical cyclones. In an interactive visualization system, the proximity and interaction of these features can be explored using temporal animations, slicing, and the inspection of related scalar variables. Since WCBs are Lagrangian structures arising from integration over a time window, we intersect their paths in space–time with the time slice selected for the view of the instantaneous tropopause and jet streams, resulting in a set of WCB positions at the time instance of the jet. By spatially filtering these positions by their proximity to jets, we identify locations at which the structures are close to each other. Using our interactive tool, multiple cases are studied and interpreted, including the acceleration of jets in the vicinity of WCBs, the movement of jets, the path of jets along tropopause folds, as well as splitting and merging events of multiple jets at the tropopause. We evaluate the parameter sensitivity and the performance of the jet stream extraction. The feature extraction pipeline opens new opportunities for further research in atmospheric sciences, and the visual analysis tool sheds light on three-dimensional processes that are difficult to grasp in 2-D slices. In summary, we contribute

- an integration-based jet core extraction algorithm that takes a predictor–corrector approach (Banks and Singer, 1994) to extract longer jet stream core lines as approximate ridge lines in the wind magnitude field, while allowing the feature lines to be regularized to align with the wind vector field;
- an automatic extraction of locations at which jet streams split or merge, which are classified based on the integration direction of the jets; and
- an interactive visualization of the extracted line geometry, which enables us to study situations where WCBs

approach a jet, as well as jet splits and merges at the folds of the tropopause.

The paper is structured as follows. Section 2 places the work among related work and explains relevant meteorological concepts that later inform the feature extraction. Section 3 introduces our novel predictor–corrector-based jet stream extraction algorithm, compares the approach with a local jet core extraction, and studies the performance and parameters of the proposed method. Section 4 integrates the jet core extraction into an interactive visualization system that allows the user to study the co-occurrence of jets with other meteorological features. In Sect. 5, the jet stream cores are visualized along warm conveyor belts and the tropopause to study the behavior of jets in the vicinity of other meteorological structures, e.g., tropopause folds. Section 6 concludes the work and outlines opportunities for further research.

2 Meteorological concepts

We begin with a brief introduction of the meteorological background and a summary of recent work on the visualization of meteorological features. For a comprehensive introduction to meteorological visualization, we refer to Rautenhaus et al. (2018).

2.1 Potential vorticity

Potential vorticity (PV) is a scalar quantity that measures the rotation of the air enclosed between two isolevels of potential temperature. It is a common diagnostic tool, as it is preserved during advection in adiabatic and frictionless flow conditions. Following Hoskins et al. (1985), we use potential vorticity PV, here defined for all quantities in isobaric coordinates, i.e., in pressure levels:

$$PV = -g \cdot (f \cdot \mathbf{k} + \nabla \times \mathbf{v}) \cdot \nabla \theta, \quad (1)$$

where g denotes the acceleration of gravity, $f = 2 \Omega \sin(\phi)$ is the Coriolis parameter, with $\Omega = 7.29 \times 10^{-5} \text{ rad s}^{-1}$ being the angular velocity of the Earth, ϕ denoting latitudes, and θ being the potential temperature. PV is measured in potential vorticity units (pvu) where $1 \text{ pvu} = 10^{-6} \text{ K m}^2 \text{ kg}^{-1} \text{ s}^{-1}$. Recently, Bader et al. (2020) extracted and visualized banners of potential vorticity, detaching from orographic mountain peaks.

2.2 Tropopause

The tropopause is the atmospheric boundary between the troposphere and the stratosphere (Holton et al., 1995; Stohl et al., 2003). The tropopause can exist anywhere between 70 hPa (around 18 km) and 400 hPa (around 6 km; cf. Dameris, 2015) and might regionally drop even lower (Lillo et al., 2021). The tropopause altitude is generally highest in the tropics and lowest near the poles, and drops sharply

across the subtropical jet. Unlike its common illustration in text books, it is far from being a smooth surface. Distinct structures, such as tropopause folds and stratospheric intrusions, frequently occur and give the tropopause a complex 3-D geometry (Danielsen, 1968; Shapiro, 1980; Škerlak et al., 2015). These structures can have an impact on a wide range of weather phenomena on the Earth's surface (Nielsen-Gammon, 2001). For instance, the evolution of surface cyclones is often associated with, or even triggered by, localized perturbations of the tropopause. Based on the potential vorticity, we seize the dynamic definition of the tropopause, as it captures complex perturbations of the troposphere–stratosphere interface. To define the tropopause, different thresholds of PV isosurfaces are used, typically between 1 and 5 pvu (Highwood et al., 2000; Schoeberl, 2004; Kunz et al., 2011; Dameris, 2015), depending on the region and the analysis task. We refer to Nielsen-Gammon (2001) for visualizations of 20 years of tropopause data, defined in terms of potential vorticity, and to Škerlak et al. (2015) for the subtleties in extracting the dynamical tropopause from numerical weather prediction (NWP) data.

2.3 Jet streams

Jet streams are fast and coherent air streams in the upper troposphere and lower stratosphere, which are hundreds of kilometers wide and only a few kilometers thick. The center of the jet stream, which is called the “jet core”, often exceeds 50 m s^{-1} and can occasionally reach wind magnitudes of 100 m s^{-1} (Koch et al., 2006; Schiemann et al., 2009; Ahrens and Henson, 2018). Jet streams and their variation are of high interest, (cf. Manney et al., 2014; Manney and Hegglin, 2018), for example, in relation to extreme weather events (Harnik et al., 2016). By the definition of the World Meteorological Organization (WMO), the jet stream is defined as “Flat tubular, quasi-horizontal, current of air generally near the tropopause, whose axis is along a line of maximum speed and which is characterized by great speeds and strong vertical and horizontal wind shears” (WMO, 1992). The heart of the jet stream, the jet core, is defined as the “Line along which the wind speeds are maximal both in the vertical and in the horizontal” (WMO, 1992).

Several approaches have been developed to automatically extract jet streams; cf. Maher et al. (2019) for a comprehensive overview. A common approach is to threshold the wind magnitude in a certain height range, as, for example, done by Limbach et al. (2012) and Martius (2014). An additional constraint is the assumption that the flow is oriented eastwards, cf. Schiemann et al. (2009). Alternatively, Archer and Caldeira (2008) locally considered mass and mass-flux-weighted averages to detect the jets. To compute the average jet wind speed, Koch et al. (2006) counted grid points that exceed a wind speed of 30 m s^{-1} between 100 and 400 hPa. Once grid points are identified that belong to jet cores, they can be further classified into different types of jets. The most

important ones being the polar and subtropical jet. This classification, however, is not trivial, since there is a continuous spectrum of jet characteristics (Lee and Kim, 2003; Manney et al., 2014, 2021; Winters et al., 2020). Pena-Ortiz et al. (2013) noted that attempting to distinguish polar and subtropical jets by latitude was commonly unsuccessful; Manney et al. (2011, 2014) found that using a simple latitude criterion was only useful for very broad climatological studies, and Manney and Hegglin (2018) introduced a more physically based method of distinguishing subtropical and polar jets based on tropopause height changes across the jet region. Winters et al. (2020) (and references therein) distinguish subtropical and polar jets by identifying them in different isentropic layers and show clear instances of them merging into jets with hybrid characteristics. Manney et al. (2011, 2014) identified sectional extrema in wind speed above 40 m s^{-1} inside latitude–altitude slices. If more than two local extrema appeared within the 30 m s^{-1} isocontour at a distance of more than 15° latitude apart or when the wind speed between the two local extrema drops by more than 25 m s^{-1} , the extrema were considered to be separate jet stream cores. Spensberger et al. (2017) identified upper-tropospheric jet core lines as locations with vanishing wind shear orthogonal to the wind direction and applied the approach to study jet variability on the Northern and Southern Hemispheres (Spensberger and Spengler, 2020). Maher et al. (2019) introduced the tropopause gradient method, which extracts jet cores by detecting turning points in the potential temperature observed along the 2 pvu isocontour. Winters et al. (2020) investigated polar-subtropical jet superpositions. Kern and Westermann (2019) studied clustering methods for ensembles of jet core lines.

Most of the methods above assume certain characteristics of the jet, for example, that the jet moves from west to east, or that it is continuous (Barton and Ellis, 2009). Kern et al. (2017) developed an approach which does not assume such characteristics and detects the jet at all levels and directions equally. By defining a local coordinate system that is composed of the horizontal wind direction $s = (u, v, 0)$ (with u being oriented eastward and v being oriented northward), the normal direction $n = (-v, u, 0)$ and the vertical axis $k = (0, 0, 1)$, jet core lines appear as sectional extrema of the horizontal velocity magnitude $s(\mathbf{x}) = \|s\|$ in the n – k plane by intersecting the two isosurfaces:

$$\frac{\partial s}{\partial n} = 0 \quad \frac{\partial s}{\partial z} = 0, \quad (2)$$

which are further filtered by an eigen-analysis of the Hessian of $s(\mathbf{x})$. While Kern et al. (2017) used a specialized variant of the marching cubes algorithm (Ljung and Ynnerman, 2003) to find solutions to the implicit equations in Eq. (2), we rephrase this problem for later comparison into a standard parallel vectors (Peikert and Roth, 1999) problem for which several local (Peikert and Roth, 1999), integration-based (Van Gelder and Pang, 2009; Weinkauff

et al., 2011) and implicit solvers (Witschi and Günther, 2020) exist, cf. Günther and Theisel (2018):

$$\begin{aligned} \begin{pmatrix} \partial s / \partial \mathbf{n} \\ \partial s / \partial z \\ 0 \end{pmatrix} \parallel \begin{pmatrix} 0 \\ 0 \\ 1 \end{pmatrix} &\Leftrightarrow \begin{pmatrix} \partial s / \partial \mathbf{n} \\ \partial s / \partial z \\ 0 \end{pmatrix} \times \begin{pmatrix} 0 \\ 0 \\ 1 \end{pmatrix} = \begin{pmatrix} 0 \\ 0 \\ 0 \end{pmatrix} \\ &\Leftrightarrow \begin{pmatrix} \partial s / \partial z \\ \partial s / \partial \mathbf{n} \\ 0 \end{pmatrix} = \begin{pmatrix} 0 \\ 0 \\ 0 \end{pmatrix}. \end{aligned} \quad (3)$$

The symbol \parallel denotes the parallel vectors operator (Peikert and Roth, 1999), which receives two vector fields as input and produces the set of points at which the two given vector fields are parallel. The two vectors are parallel if their cross product vanishes to zero. Applying the cross product results in three equations: the two equations from Eq. (2) and $0 = 0$. Since this is a local feature extraction method, the resulting jet cores are often short and have to be heuristically connected. Especially in combination with a wind magnitude filter, the lines can decay into pieces if no global ideal threshold exists. This problem can be reduced by prior smoothing of the fields, which, however, affects the precise location of the feature. Rather than extracting lines locally, we choose an integration-based approach to extract the jet core lines using a predictor–corrector algorithm (Banks and Singer, 1994). Our aim is to not only extract core-line segments but also to keep track of the connections between them. We do this by allowing the jet core to be weaker than the strength threshold for a limited number of integration steps. In addition, we identify splitting and merging events of jet core lines.

2.4 WCBs

Cyclones are important components of the climate system. They are responsible for a major fraction of the meridional moisture and heat transport, and produce most of the precipitation in the midlatitudes (Wernli and Schwierz, 2006; Schultz et al., 2019). Further, they clean the atmospheric boundary layer from aerosols and pollution (Eckhardt et al., 2004). The WCB is one out of three important air streams found in extratropical cyclones. The others are the dry intrusion (Raveh-Rubin, 2017) and the cold conveyor belt (Madonna et al., 2014). The WCB is responsible for strong cloud formation, precipitation as well as modifying the potential vorticity (Madonna et al., 2014). Further, WCBs influence the evolution of cyclones. For example, a strong WCB next to an extratropical cyclone can hint at rapid storm development (Binder et al., 2016). Also they can be used to characterize the geographical distribution of cyclones (Eckhardt et al., 2004). They are also highly relevant to numerical weather prediction, because they can be a major source and magnifier of forecast uncertainty (Rodwell et al., 2018). WCBs usually originate in the moist subtropical marine boundary layer between 20 and 45° latitude (Wernli, 1997). In the Northern Hemisphere, most of the WCBs appear close to a center of a cyclone and they are more com-

mon in winter than in summer. In the Southern Hemisphere, the WCBs vary less and there are no WCBs over polar regions (Madonna et al., 2014). To find WCBs, a Lagrangian selection criterion can be used based on the fact that WCBs ascend strongly, typically by more than 600 hPa with 48 h. Similar criteria have been used by Wernli (1997), Eckhardt et al. (2004) and Madonna et al. (2014). For example, Eckhardt et al. (2004) extracted 15 years of WCB trajectories starting at 500 m above ground level. They extracted only the trajectories which in 2 d traveled northward and ascended at least 60 % of the zonally and climatologically average tropopause height. Rautenhaus et al. (2015a) estimated the probability for the existence of WCBs from particle trajectories in an ensemble of flows and visualized WCBs in 3-D. In addition to the slantwise and slow ascent, recent studies considered the rapid, convective transport that can be embedded in the WCB (Oertel et al., 2019).

3 Integration-based jet stream extraction

3.1 Data

For our analysis, we used the ERA5 reanalysis data (Hersbach et al., 2020), provided by the European Centre for Medium-Range Weather Forecasts (ECMWF). We use hourly data from 1 September 2016 at 00:00 UTC to 31 October 2016 at 23:00 UTC, which coincides with the North Atlantic Waveguide and Downstream Impact Experiment (NAWDEX) (Schäfler et al., 2018) field campaign. The spatial data are stored on a regular grid with dimensions $720 \times 361 \times 98$ for three-dimensional fields and 720×361 for two-dimensional fields. The vertical dimension is given on hybrid sigma–pressure levels (Eckermann, 2009), spanning a range from 27.8 hPa to 1039.9 hPa. For jet core extraction in our 2-month data set, we consider the range from 190 to 350 hPa, in which the jets can be expected. Jets may very well occur outside of this range for other time periods, both below and above our chosen thresholds (e.g., Manney et al., 2014). Thus, depending on the spatial and temporal region of interest, the thresholds should be adapted. The horizontal grid spacing is 0.5° in lat/long and for computational convenience, we resampled the height levels onto uniformly spaced 10 hPa pressure levels. For our data, the regridding produces approximately 10 times more vertical samples, which consumes additional memory. This could be avoided by working directly on the hybrid model-level data, which requires adjustments in the calculation of partial derivatives and in the interpolation. In principle, it would also be possible to perform the jet stream core-line extraction in other coordinate systems, for example, in isentropic coordinates where the vertical levels have equal potential temperature.

We refer the interested reader to the works of Kern et al. (2017) and Kern and Westermann (2019), who studied jets in the same time period, including an ensemble analysis

which is another practical application of explicitly extracted jet stream core lines.

3.2 Feature extraction

Kern et al. (2017) defined jet core lines as ridge lines of the wind magnitude field.

For numerical weather data, local Hessian-based ridge detectors (Eberly, 1996) pose numerical challenges in the second-order derivative estimation and the subsequent eigenanalysis, as pointed out by Kern et al. (2017), who locally extracted the ridge line with a first-order method as described earlier in Eq. (2). Especially in a low vertical resolution in the upper atmospheric layers, a pure extremal line definition can suffer from numerical problems, as shown in Fig. 1 (red lines). Since local methods further require heuristics to connect line segments, we apply the predictor–corrector algorithm by Banks and Singer (1994), where we change the underlying scalar and vector field. With this, ridge lines are calculated incrementally by alternating between predictions and corrections. The predictor–corrector approach serves two purposes. First, it allows tracing out those lines leading to longer connected jets. Second, by balancing between predictor and corrector steps, the trajectory can be regularized to follow wind vectors directly during feature extraction, rather than in a post-process. With this, unnaturally bending jet core lines due to discretization problems can be reduced; see Fig. 1 (blue lines).

In the following, we explain the algorithm in detail. For brevity, we omit the time parameter t in the velocity magnitude field $s(\mathbf{x})$ and the normalized wind velocity field $\bar{\mathbf{v}}(\mathbf{x}) = \mathbf{v}(\mathbf{x})/\|\mathbf{v}(\mathbf{x})\|$. We utilize a normalized field, since core lines are extracted per time step. In such an instantaneous flow, normalization results in the same streamline geometry but with more explicit control over the integration speed.

3.2.1 Initial seed points

As initial seed points in the first frame, we select all local maximal extremal points \mathbf{x}_0 of the wind magnitude field $s(\mathbf{x})$ in Fig. 2a with a wind magnitude of at least $s(\mathbf{x}_0) > 40 \text{ m s}^{-1}$ between 350 hPa (around 8 km from the Earth’s surface) and 190 hPa (around 12 km from the Earth’s surface). We chose this region and the wind speed threshold empirically for our data set. Note that we use discrete extremal points, i.e., grid points for which all neighboring grid points have a smaller value, in order to avoid the numerical estimation of derivatives. The seed points are shown in Fig. 2b. All seed points are sorted in descending order by the wind magnitude; i.e., we begin our further processing with the global maximum. From each seed point, the jet core line is traced forward and backward, as explained in the following.

3.2.2 Prediction

Assuming that the flow direction is a fair estimate for the jet core-line tangent, the prediction estimates the next point $\hat{\mathbf{x}}_{i+1}$ of the jet core line in the direction of the velocity field $\bar{\mathbf{v}}(\mathbf{x})$:

$$\hat{\mathbf{x}}_{i+1} = \mathbf{x}_i + h \cdot \bar{\mathbf{v}}(\mathbf{x}_i), \quad (4)$$

with h being the integration step size for which we use the grid spacing. In practice, we take a fourth-order Runge–Kutta step instead of an Euler step. The velocity $\bar{\mathbf{v}}(\mathbf{x}_i)$ at point \mathbf{x}_i is trilinearly interpolated from the discrete grid storing the velocity values. The flow direction is not only an estimate for the next vertex location; it also serves as regularization to align lines with the wind vector field.

3.2.3 Correction

Since $\hat{\mathbf{x}}_{i+1}$ might not be precisely on the ridge line of the wind magnitude field, a correction is applied, which moves the point in the plane orthogonal to the flow direction back towards the ridge line:

$$\mathbf{x}_{i+1} = \hat{\mathbf{x}}_{i+1} + h \cdot \left(\nabla s(\hat{\mathbf{x}}_{i+1}) - \bar{\mathbf{v}}(\hat{\mathbf{x}}_{i+1}) \cdot \nabla s(\hat{\mathbf{x}}_{i+1})^T \bar{\mathbf{v}}(\hat{\mathbf{x}}_{i+1}) \right), \quad (5)$$

which is iterated until a maximal number of iterations is reached. The number of correction iterations determines how closely the extracted jet stream will follow a ridge line of the wind magnitude field (high number of iterations) or be tangential to the wind field (low number of iterations). We show different choices later in Sect. 3.4. In this procedure, the velocity field is normalized, such that the traveled distance in both the prediction and the correction is independent of the wind speed, and is instead controlled by the number of prediction steps $n_{\text{predSteps}}$ and the number of correction steps $n_{\text{corrSteps}}$ in each predictor–corrector iteration.

3.2.4 Termination

Iterating the predictor and corrector step incrementally traces out the jet core lines. We terminate the jet core-line tracing under three conditions: (1) the wind magnitude $s(\mathbf{x})$ remained below a user-defined threshold for more than n prediction steps (to admit line segments that fall below the threshold only for a short amount of time); (2) the angle between two consecutive line segments is larger than 60° , which is a quality criterion adapted from Kern et al. (2017) to prevent unnatural bending; (3) the new predictor step comes too close to an already computed jet core line. The latter avoids the duplicate tracing of jet core lines and allows recording split and merge events as explained below. In contrast, Bader et al. (2020) applied an agglomerative hierarchical clustering to remove duplicates, which required a suitable line distance measure and distance threshold.

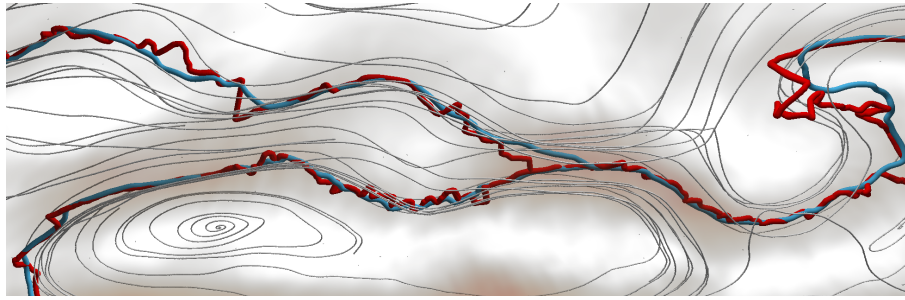


Figure 1. Extremal lines (red lines) of the wind magnitude are sensitive to the data discretization and thus do not follow the streamlines (gray lines) of the wind field. In contrast, our jet core lines (blue lines) balance between extremal lines and flow alignment. All lines are traced in 3-D and may therefore intersect on the viewport. Locations with wind speed between 10 and 40 m s⁻¹ are highlighted with gray-red color in the background, showing that jet core lines reside in high velocity regions. The data here are for 1 September 2016 at 00:00 UTC.

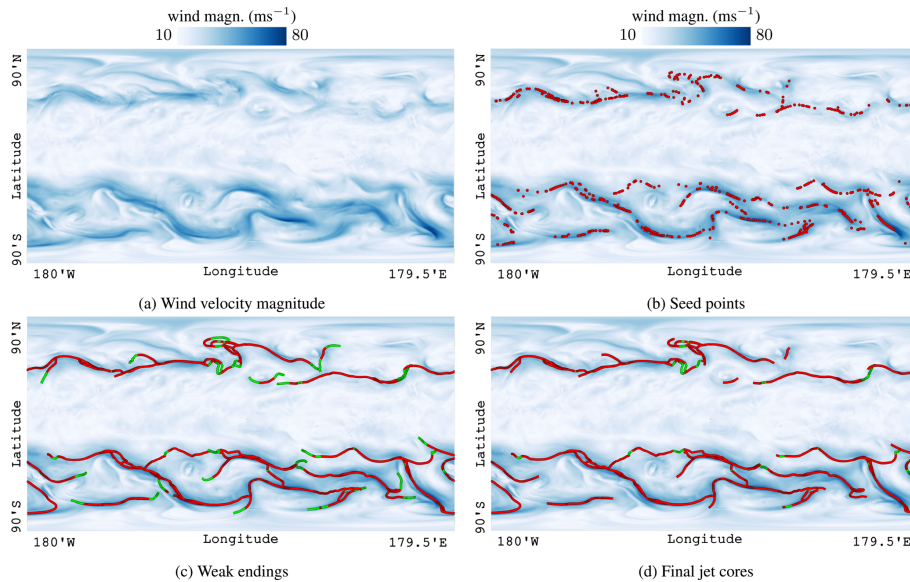


Figure 2. Panel (a) shows a slice of the wind magnitude field. White indicates low wind speed; blue indicates high wind speed. Panel (b) is the same as (a), overlaying seed points in red. Panel (c) shows predictor–corrector results with weak endings in green. Panel (d) shows the final result, after the weak endings have been removed. Finally, green segments denote regions at which the velocity magnitude threshold was temporarily not reached. The data here are for 8 September 2016 at 12:00 UTC.

3.2.5 Split and merge detection

The previously mentioned third termination criterion is used to locate coordinates at which jet streams split or merge. If the new point is closer than a user-defined threshold to an already existing jet stream, we record the event. The search for the closest point on the previously traced jet core lines is accelerated by using a *kd* tree and performing a nearest-neighbor search, for which we used the library nanoflann (Blanco and Rai, 2014). Empirically, we applied a horizontal distance threshold of 1° latitude or longitude and a vertical distance below 5 hPa as threshold. The type of event (split or merge) is identified by the line orientations. If a jet stream integration approaches an existing jet stream while doing a forward integration, then we mark this location as

a merge point. If the jet stream approaches an existing jet stream during a backward integration, then a split point is found.

3.2.6 Pruning

Since the predictor–corrector algorithm tracks jet core lines even after they fall under the wind magnitude threshold, all lines have an ending which is below the jet stream threshold τ_{wind} . In Fig. 2c, this is indicated with green lines, whereas the red lines actually belong to the jet core. We remove those weak endings in a post-process by pruning end points until the velocity magnitude threshold of the last point is reached; see Fig. 2d.

3.2.7 Temporal tracking

In the first frame, we extracted local wind magnitude extrema above the wind magnitude threshold as potential seed points, sorted them by the wind magnitude, and incrementally applied the predictor–corrector algorithm for one seed point at a time in descending order. For all subsequent frames, we construct our seed point set differently. For all jet core lines of the previous frame, we first extract the local wind magnitude extrema on the jet cores to form candidates. Each of these points performs a local gradient ascent in the next time step to find a nearby local maximum. This way, the seed point set remains temporally more coherent than when it was created anew. Seed points are removed if the new local maximum does not reach the wind magnitude threshold anymore. To not miss jets that are forming in the next time step, we insert local wind magnitude extrema in regions not covered by jets. In Fig. 3, four time steps of an animation are shown, which display the movement of jets and their temporal evolution. We refer to the accompanying video for the full animation.

3.3 Comparison with local method

In numerical simulations, the domain is discretized onto a grid, composed of cells in which attributes are interpolated. Local line extraction methods solve for lines in three steps (Peikert and Roth, 1999). First, intersection points with the cell boundaries are computed numerically per cell. Second, the intersection points are connected to form line segments within the cells, which may fail if intersection points were missed or are duplicated for numerical reasons. Third, the line segments are connected to continuous lines when the end points of two segments are close enough to each other (within a threshold) and when the tangent directions at the end points align (up to a certain threshold). The result of this last operation is order dependent, depends on the numerical accuracy of the first step and is dependent on thresholds. Figure 4a gives an example of the parallel vectors formulation in Eq. (3), which produces many small disconnected line pieces, depending on the threshold choices. Further, the lines are restricted to regions in the domain with a velocity magnitude larger than 40 m s^{-1} . In order to produce clean results, local methods often require parameter tuning, filtering (for example, by line length), or extensive smoothing of the input fields. Instead, our integration-based approach in Fig. 4b can naturally grow the lines in direction of the vector field, allowing us to construct long connected jet core lines.

3.4 Performance and parameter study

In this section, we analyze the performance and discuss parameter choices. The system on which we run the measurements contains an AMD Ryzen 9 3900X CPU. In the pre-process, we resample the data to equidistant pressure levels 10 hPa apart ($720 \times 361 \times 104$), which takes on average 28.2 s

per time step and generates 1.62 GB additional disk space per time step. The WCB pre-processing for all time steps takes 213.6 s and generates 0.86 GB additional disk space. On average, the extraction time of jet stream core lines takes about 10 s per simulation time step. For a total of 2 months of hourly simulation data, this leads to a pre-processing time of 12 h for the whole data set and an additional disk space usage of 2.37 TB, compared to the original data set size of 903 GB.

The default parameters of the jet core extraction and the performance measurements can be seen in Table 1 for the time step on 1 September 2016 at 00:00 UTC. Increasing τ_{wind} , i.e., the wind magnitude threshold for being classified as jet stream, leads to fewer jet core lines, because fewer vertices meet the filter criterion. In contrast, if chosen smaller, more vertices will pass the threshold filter and will be recognized as belonging to jet core lines. Increasing $n_{\text{stepsBelowThresh}}$, i.e., the number of integration steps a core line can be below the velocity magnitude threshold, leads to more connected structures. In Fig. 5, we demonstrate the impact of varying the number of prediction steps $n_{\text{stepsBelowThresh}}$ a jet core line is allowed to remain under the wind speed threshold. When setting the value too high, lines might be found that are not actually jets. Setting $n_{\text{predSteps}}$, i.e., the number of predictor steps per iteration, too high leads to inaccurate results, as it takes the predictor too far away from the ridge line, making it more difficult for the corrector. A single predictor step is recommended. The parameter that influences the performance the most is $n_{\text{corrSteps}}$, the number of corrector steps performed in an iteration. When chosen too small, less lines merge, which increases the computation time. Likewise, a too-large number, i.e., when converging onto ridge lines, causes computation overhead. The number of corrector iterations $n_{\text{corrSteps}}$ in the predictor–corrector procedure allows the user to balance how closely the jet stream follows a wind magnitude ridge line (high number) or the wind vector field (low number). In Fig. 6, we display the resulting jet core lines for different numbers of corrector steps, i.e., different degrees of regularization. A cross section of the velocity magnitude scalar field shows that with regularization the curves pass close to the ridge lines, but they result in smoother lines instead. The accompanying video contains animations of the cross-section plane, showing that the regularized curves show reasonable agreement with the sectional extrema.

4 Interactive visualization system

We implemented our integration-based jet core-line extraction in an interactive visualization system in order to visually analyze the jet streams in the context of warm conveyor belts and the tropopause. Our system is implemented using the Visualization Toolkit (VTK) (Schroeder et al., 2006).

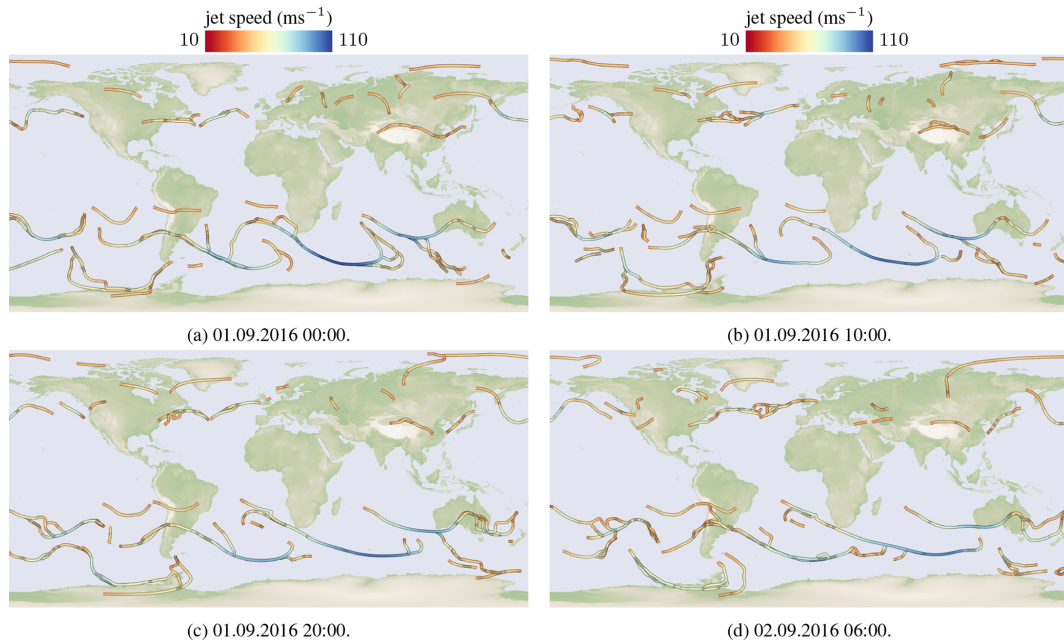


Figure 3. Temporal tracking of the jet stream. Here, shown for four time steps with an integration step size of 10 h between 1 September 2016 at 00:00 UTC and 2 September 2016 at 06:00 UTC. Especially the fast-moving wind speeds (blue structures) are tracked coherently over time.

Table 1. The extraction time in seconds when changing one parameter value while keeping the others fixed, listed here for the default parameters and two variations from the default parameters. Increasing $n_{\text{stepsBelowThresh}}$ prolongs the integration duration since longer lines emerge. Increasing $n_{\text{predSteps}}$ per iteration traces out the jet lines with less iterations. The smaller τ_{wind} (in m s^{-1}), the more lines are traced. With lower $n_{\text{corrSteps}}$, less jets merge, causing higher tracing cost. For higher $n_{\text{corrSteps}}$, the runtime increases linearly due to more steps.

Parameter	Parameter value			Extraction time (s)		
	Default	Variation 1	Variation 2	Default	Variation 1	Variation 2
τ_{wind}	40	30	50	10.1	12.2	8.2
$n_{\text{stepsBelowThresh}}$	100	0	1500	10.1	9.6	11.6
$n_{\text{predSteps}}$	1	2	5	10.1	8.8	9.8
$n_{\text{corrSteps}}$	5	1	12	10.1	13.0	12.5

4.1 Overview

The visual analysis of meteorological data is generally challenging, since the data are three-dimensional and time dependent, and contain a number of variables that interact with each other. Furthermore, numerical weather simulations are produced at increasingly higher resolution, resulting in several TB per case. Because the time series data are far too large to be held in memory, it is necessary to calculate features, such as the tropopause geometry, warm conveyor belt trajectories, and jet stream core lines once in a pre-process. The resulting geometric descriptions of the meteorological features are not only valuable for interactive visualization; they can also be input to traditional data analysis pipelines. To increase the compatibility with the accustomed workflows, we implemented the feature extraction in a command line tool, including the computation of the jet core lines, warm con-

veyor belts, and the tropopause. The code is available in the Supplement. Subsequently, the features are passed on to an interactive analysis tool, with which we explore jet stream core lines for multiple use cases:

- We show a case in which a warm conveyor belt outflow feeds a jet stream, thereby accelerating it.
- We demonstrate that our extracted jet streams align well with flanks of the tropopause.
- We visualize a setting in which the outflow of a WCB coincides with a displacement of a jet.
- We display the tropopause at locations where jet streams split and merge.

To this end, the tool supports the combined visualization of features, the computation of derived properties, and interac-

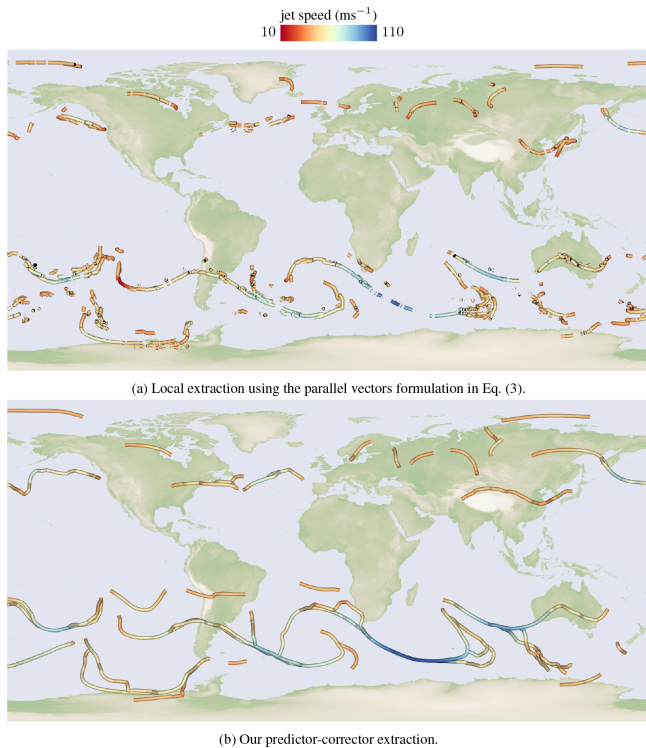


Figure 4. (a) Local extraction methods on unsmoothed data may lead to spurious jet core lines that need substantial post-processing and filtering. (b) Our method results in continuous curves. Extraction results are shown for 1 September 2016 at 00:00 UTC.

tive filtering operations. An overview of our pipeline is provided in Fig. 7. Next, we formally define the meteorological features and describe the components of the interactive visualization system.

4.2 Feature extraction

Let $\mathbf{v}(\mathbf{x}, t) : \mathbb{R}^3 \times \mathbb{R} \rightarrow \mathbb{R}^3$ be the time-dependent wind vector field. Its spatial coordinates $\mathbf{x} = (\phi, \lambda, p) \in \mathbb{R}^3$ are measured in latitude, longitude, and pressure. The wind velocity components are in m s^{-1} (horizontally) and Pa s^{-1} (vertically). The thresholds used in the definitions have been chosen empirically and can be adjusted depending on the analysis task.

4.2.1 Jet stream core line

The jet stream core lines are extracted by the algorithm described in Sect. 3. In the following, we denote jet core lines in the time-dependent horizontal wind magnitude field $s(\mathbf{x}, t) = \|(u(\mathbf{x}, t), v(\mathbf{x}, t))\|$ as instantaneous curves $\mathbf{c}(\tau) : \mathbb{T} \rightarrow \mathbb{R}^3$, arc length parameterized by $\tau \in \mathbb{T} \subset \mathbb{R}$. Since these lines evolve over time t , we introduce a time-dependent set $\mathcal{C}(t) = \{\mathbf{c}_i(\tau)\}$, which contains all jet core lines for a given time t , where i is the index of the line.

4.2.2 Tropopause

We define the tropopause to be the largest connected surface composed of isosurfaces with isovalue 2 and -2 pvu of the potential vorticity field on the Northern Hemisphere and Southern Hemisphere, respectively. Other choices for the PV thresholds are imaginable (cf. Highwood et al., 2000; Schoeberl, 2004; Kunz et al., 2011). Further, the pressure was required to be below a threshold of 740 hPa to remove false positives near the ground. Note that this pressure threshold is by no means a general constant. For example, Lillo et al. (2021) identified tropopause droppings well above the threshold at intense sub-synoptic-scale events. Formally, the time-dependent tropopause is expressed as $\mathcal{T}(t) \subset \mathbb{R}^3$ with

$$\begin{aligned} \mathcal{T}(t) = & \{ \mathbf{x} : P(\mathbf{x}, t) = +2 \text{ pvu} \wedge \phi > 0 \wedge p < 740 \text{ hPa} \} \\ & \cup \{ \mathbf{x} : P(\mathbf{x}, t) = -2 \text{ pvu} \wedge \phi < 0 \wedge p < 740 \text{ hPa} \}, \end{aligned} \quad (6)$$

where $P(\mathbf{x}, t)$ denotes the PV field. For procedures on how to address the sign flip at the Equator, we refer to Schoeberl (2004); Manney et al. (2011) for a formulation based on an isentropic isosurface. In our work, we extracted the PV isosurfaces for the Northern Hemisphere and Southern Hemisphere separately.

4.2.3 WCBs

Formally, we describe the set of WCB trajectories $\mathcal{W} = \{\mathbf{x}(t)\}$ as the union of all path lines $\frac{d\mathbf{x}(t)}{dt} = \mathbf{v}(\mathbf{x}(t), t)$ of the wind velocity field $\mathbf{v}(\mathbf{x}, t)$ that ascend within $T \leq 48$ h more than $\Delta_p = 600$ hPa:

$$\begin{aligned} \mathcal{W} = & \left\{ \mathbf{x}(t) : \mathbf{x}(t) = \mathbf{x}_0 + \int_{t_0}^{t_0+T} \mathbf{v}(\mathbf{x}(t), t) dt \right. \\ & \left. \wedge \left(\exists \tau \in [0, T] : p(t_0) - p(t_0 + \tau) > \Delta_p \right) \right\}. \end{aligned} \quad (7)$$

To form \mathcal{W} , the trajectories are seeded from a dense space-time grid with initial coordinates $\{(\mathbf{x}_0, t_0)\}$ near the ground, using a horizontal grid spacing of 80 km, 14 equidistant vertical levels between 1050 and 790 hPa, and a temporal spacing of 6 h. Trajectories are numerically integrated using a fourth-order Runge–Kutta integrator.

4.2.4 Combining Eulerian and Lagrangian features

Note that the tropopause surface $\mathcal{T}(t)$ and the set of jet stream core lines $\mathcal{C}(t)$ depend on the observation time t . This means, they are Eulerian features; i.e., they are computed per time slice t . The WCB trajectories in \mathcal{W} , on the other hand, exist over multiple time steps, i.e., these are Lagrangian features. Care must be taken when visualizing Eulerian and Lagrangian features together in space, since points on these two

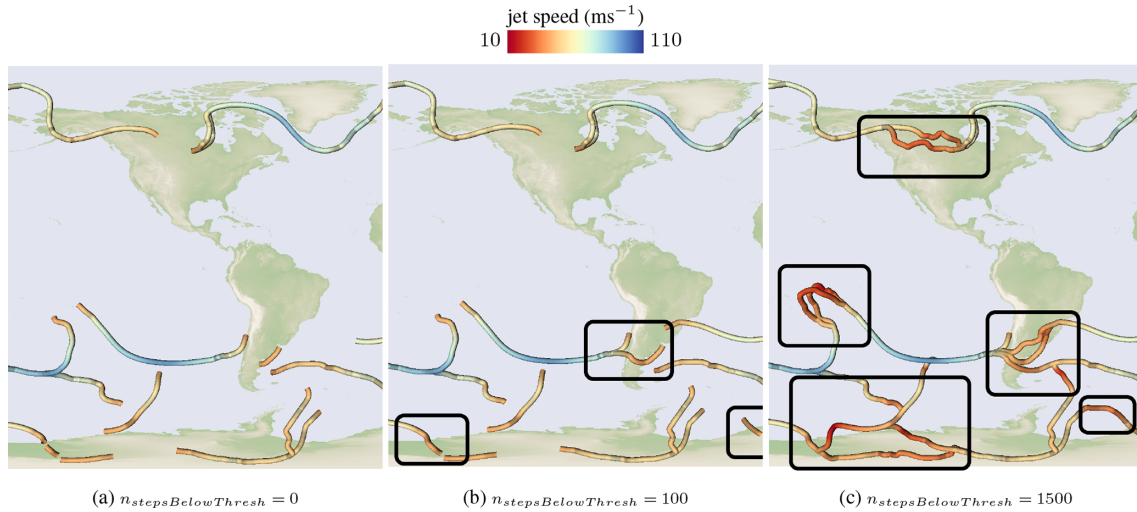


Figure 5. Increasing the number of prediction steps, a jet core might remain below the wind magnitude threshold, resulting in longer connected jet core lines. The data here are for 11 September 2016 at 15:00 UTC.

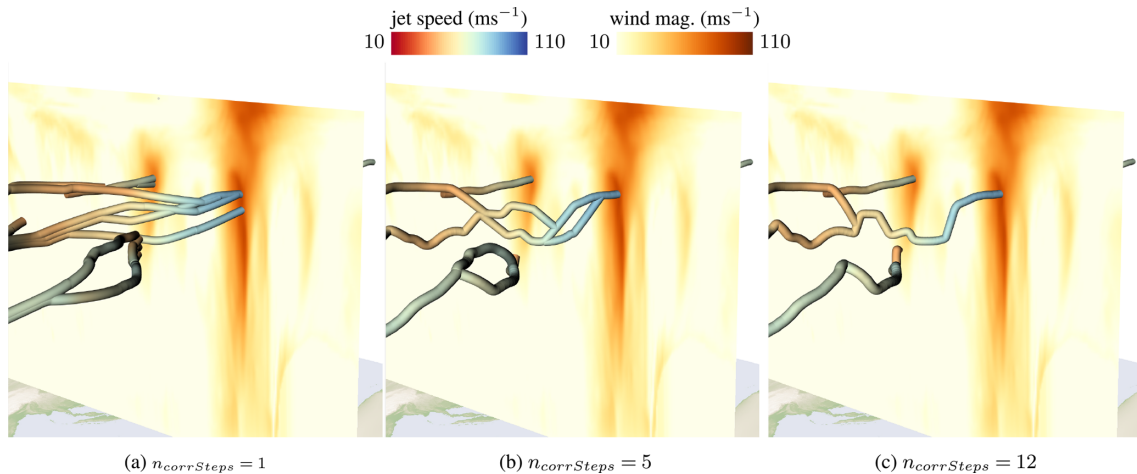


Figure 6. Comparison of jet core lines for varying number of correction iterations. The higher the number, the closer the line follows a ridge line, as proposed by Kern et al. (2017), which might exhibit higher curvature. Lowering the number of corrector iterations smooths the line. A cross section of the wind magnitude field shows how well the extracted core lines pass through sectional extrema. The data here are for 11 September 2016 at 15:00 UTC.

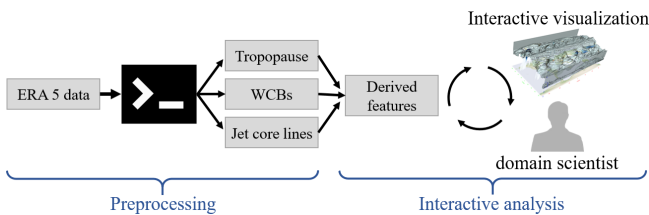


Figure 7. Our pipeline consists of two steps: a pre-processing that calculates the tropopause, WCB, and jet core-line geometries using a command line tool, and an interactive analysis in which the user interactively explores the correlation of those features in 3-D.

structures might be far apart in time, potentially leading to wrong conclusions. Since the dense set of WCB trajectories is furthermore prone to generate visual clutter, we extract the locations of WCB trajectories that exist at a certain time t , which results in a set of points $\mathcal{W}(t)$:

$$\mathcal{W}(t) = \{ \mathbf{x}(\bar{t}) \in \mathcal{W} : \bar{t} = t \}. \tag{8}$$

This point set contains all locations that are reached by any of the WCB trajectories at a certain time t , regardless of their seed time. Since the complete set of WCB points at a certain time t is still too dense, and since we are primarily interested in the interaction of WCBs and jets, we filter this point set based on the proximity to a jet in Eq. (9). For this, we empirically use a horizontal distance threshold of 15° latitude–longitude

and a vertical pressure difference of at most 50 hPa:

$$\mathcal{W}^*(t) = \left\{ \mathbf{x}(\bar{t}) \in \mathcal{W} : \bar{t} = t \right. \\ \wedge (\exists \mathbf{c}(\tau) \in \mathcal{C}(t) : \|\mathbf{c}(\tau) - \mathbf{x}(t)\| < 15^\circ \\ \wedge |p(\mathbf{c}(\tau)) - p(\mathbf{x}(t))| < 50 \text{ hPa}) \left. \right\}. \quad (9)$$

4.3 Visualization

4.3.1 Visual mapping

Rautenhaus et al. (2015b, a) developed seminal 3-D visualization methods for the analysis of jets, WCBs, and the tropopause using the framework Met.3D. In the following, we describe how we visualize jets, WCBs, and the tropopause, for which we similarly use a combination of particles, tubes, and isosurfaces. The tropopause $\mathcal{T}(t)$ is extracted as isosurface of the potential vorticity field and can be rendered semi-transparently in order to allow a view onto the structures behind it. To encode the velocity magnitude of jets $\mathcal{C}(t)$ and to convey a 3-D impression of their shape, we map the magnitude to both color and tube radius using transfer functions; i.e., color and tube radius are dependent on the magnitude. Color bars above the visualizations depict the mapping throughout the paper. The mapping to the radius is adjusted to align the resulting radius with the actual spatial extent of the jet streams. The warm conveyor belt particles $\mathcal{W}^*(t)$ at the selected time slice are rendered as magenta spheres. To encode temporal information about their motion, we display short path lines in both forward and backward time, originating from the warm conveyor belt particles; see Fig. 8b. To provide context, we add a world map with image courtesy of Reto Stockli, NASA Earth Observatory Group.

4.3.2 Viewing projections

While viewing the scene with an equirectangular mapping has many advantages, it can be beneficial to view the scene in a different projection. For example, if we want to examine parts of the jet stream that moved towards the poles. In this case, viewing the scene on a polar stereographic map gives us a more accurate picture because as soon as the jet comes close to the poles on the equirectangular map, it becomes one long tube due to distortion. However, this projection can only show either the Northern Hemisphere or the Southern Hemisphere. In addition, we provide the user with the option to view the data on a 3-D globe, conveying a correct depiction of sizes. The different projections are shown in Fig. 9. Alternatively, any other projection such as a north polar orthographic or a north polar Lambert equal-area projection would be imaginable as well.

4.3.3 User interaction

In all examples, the vertical axis (distance to ground) is scalable by the user. Further, the time slider, transfer functions of

color and radius, as well as the filtering thresholds can be interactively adjusted to explore their effect. To provide further context, image slices, isosurfaces, and direct volume renderings of additional scalar fields can be added and interactively adjusted. Figure 9 (right) gives an example of a slice showing the velocity magnitude.

5 Applications

In the following, we visualize jet stream core lines in the context of warm conveyor belts and the tropopause. The close alignment of jet core lines with folds of the tropopause is a strong indicator of the plausibility of the extracted jets Maher et al. (2019). Further, the influence of WCBs is reflected in the behavior of the jet in the case studies. We refer to the Supplement for time series animations.

5.1 Jet acceleration

In Fig. 10, we visualize how a WCB outflow that intersects with a jet stream can greatly accelerate it. In Fig. 10a, we see how a WCB approaches the jet stream and in Fig. 10b, we see the situation 2 d later. We can observe a considerable acceleration of the wind speed at the jet stream core. There are several reasons why these local jet maxima, so-called jet streaks, are of eminent importance in dynamic meteorology: (i) the entrance and exit regions of jet streaks are associated with an ageostrophic (vertical) circulation, which – for instance – favors lifting motion in the right exit and thus is conducive for storm development and the initiation of convection (Shapiro and Keyser, 1990). (ii) Jet streaks have also been identified in upper-tropospheric regions with substantial cross-tropopause mass fluxes; i.e., ozone-rich stratospheric air might be transported because of them from the stratosphere into the troposphere (Sprenger et al., 2003). (iii) The jet streaks themselves have a distinct life cycle that can, after their genesis, influence the flow evolution and the weather predictability far downstream of the genesis region (Cunningham and Keyser, 2002). Jet-accelerating interactions are currently a particularly active topic in WCB research. In fact, Oertel et al. (2020) and Blanchard et al. (2021) recently identified negative-PV structures produced in convective ascents embedded in a WCB that then locally accelerated the jet.

5.2 Jets at the tropopause

According to Winters et al. (2020); Maher et al. (2019); Koch et al. (2006), the jet stream is dynamically linked to locations with a strong potential vorticity gradient. By the dynamic definition of the tropopause, this is where the extracted tropopause isosurface is steep. Winters et al. (2020); Maher et al. (2019); Manney et al. (2014) showed that extratropical westerly jet cores are located along the flanks of “valleys” or folds of the dynamic tropopause, i.e., where the tropopause shows substantial (vertical) excursions from

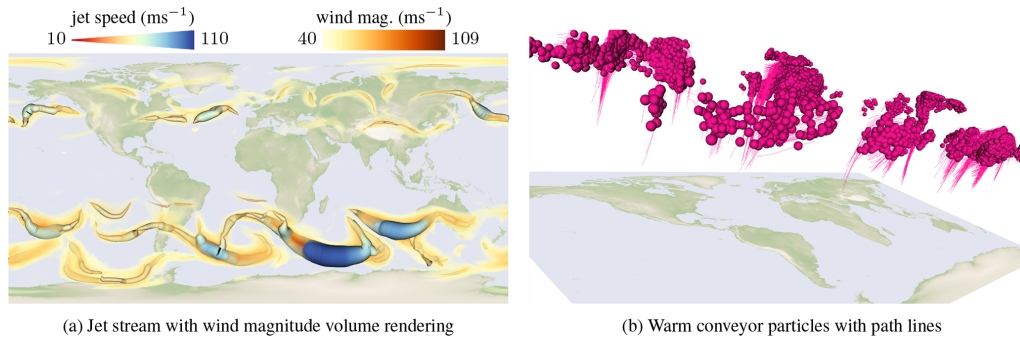


Figure 8. Jet stream core lines are rendered as tubes, with jet speed being mapped to color and radius. (a) With volume rendering of wind speed, (b) warm conveyor belt particles are shown as particles with path lines attached to convey motion.

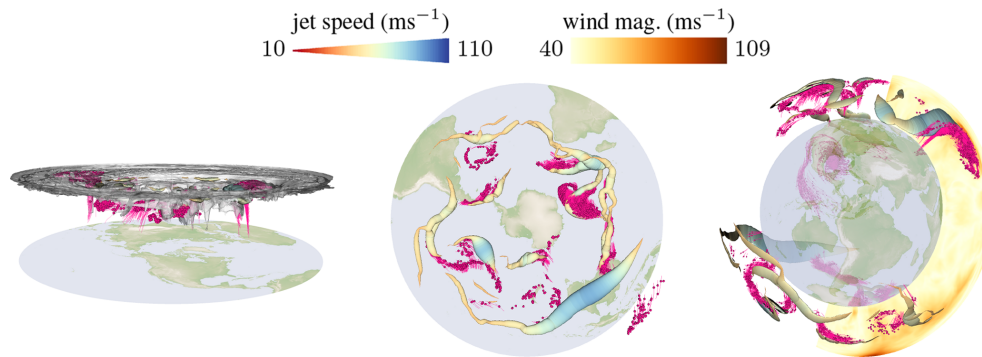


Figure 9. Interactive visualizations of acceleration, movement, and splitting and merging of jet streams. Here, polar stereographic projections of the tropopause, jet streams, and WCB outflows (magenta) for the Northern Hemisphere (left), Southern Hemisphere (middle), and a 3-D globe view with interactive volume slices (right) are shown. Jet speed is mapped to tube color and tube radius.

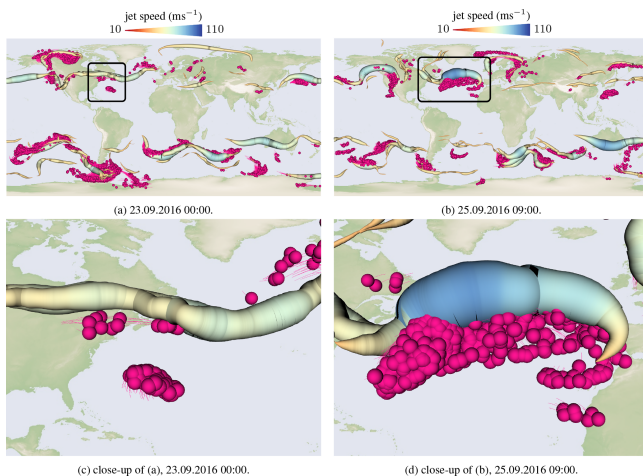


Figure 10. Visualization of jet streams $\mathcal{C}(t)$ and WCB particles $\mathcal{W}^*(t)$. Panel (a) shows a WCB outflow moving northwards in direction of the jet stream. Panel (b) shows the situation 2 d later. The WCB approached the jet stream and a considerable acceleration of the wind speed at the jet core is observable (dark blue jet). For both images, close-ups are shown in panels (c) and (d). Jet speed is mapped to tube color and tube radius.

a smooth and horizontal basic state. Figure 11 shows jet streams and the tropopause geometry using an equirectangular and polar stereographic projection. Especially in the supplemental video, the connection between jet stream and tropopause is apparent. As the tropopause evolves over time, the jet stream changes accordingly, and a smooth temporal evolution of the jets at the flank of the tropopause is a useful plausibility measure. The three-dimensional visualizations reveal not only the complicated 3-D structure of the tropopause; they also illustrate the jet stream location relative to the folds at multiple pressure levels. This allows the complex co-evolution of the two features to be studied, which would be difficult to achieve in simple isentropic or isobaric 2-D visualizations.

A 3-D view of the co-evolution may prompt further hypotheses to be investigated by means of a dynamical analysis of the physical processes involved, which might shed further light on the mechanisms governing the downstream propagation, and potential amplification, of jet (or PV) anomalies, with significant implication for weather predictability (Grams et al., 2011).

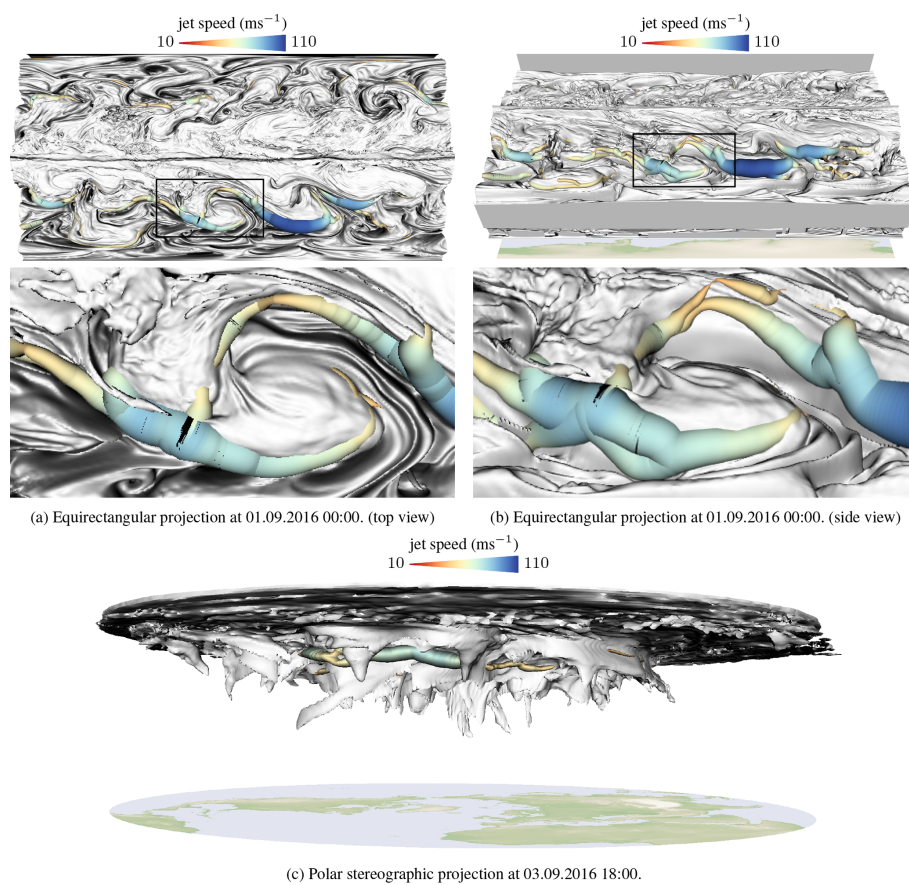


Figure 11. Interaction of jet stream and tropopause. The jet stream is located where the tropopause is steep. Jet speed is mapped to tube color and tube radius.

5.3 Jet displacement

Because the jet stream is dynamically linked to locations with a strong potential vorticity gradient (Maher et al., 2019; Winters et al., 2020; Koch et al., 2006), we now visualize WCBs, PV at 270 hPa, and the jet stream. In Fig. 12a, we see a WCB approaching the jet stream, and in Fig. 12b, we observe the situation 2 d later. We observe that a displacement of the jet stream occurs in the presence of the WCB as Steinfeld et al. (2020) found while examining the same case as shown in Fig. 12. As discussed before, WCBs can influence the jet in different ways: either they lead to local wind speed maxima (jet streaks, as in Fig. 10) or they directly displace the jet from its initial position (Oertel et al., 2020; Blanchard et al., 2021; Joos and Forbes, 2016). Often, this jet perturbation is considered in a PV perspective. This is so because WCBs transport low-PV air into upper-tropospheric levels, which in turn can help to enhance or redirect local PV gradients and jets. By considering the jet as a 3-D feature (instead of a PV gradient on a single isentropic or isobaric level), the interaction of the WCB with and the impact on the wind speed becomes more direct. A better understanding of jet displacements and accelerations by WCBs is of interest

to the NWP community, because of the high relevance for weather predictability downstream of the WCB–jet interaction (Grams et al., 2011; Rodwell et al., 2018). In fact, Davies (2015) used the term “weather chains” to highlight that upstream impacts, e.g., WCB–jet interactions in the North Atlantic, influence the weather downstream, e.g., over Europe. Currently, it is discussed whether WCBs are partly responsible for so-called forecast busts (Rodwell et al., 2013), i.e., particularly poor forecasts.

5.4 Jet split and merge

Jet streams are rarely one connected band around the planet. The jet streams can split and merge every now and then and even the polar and the subtropical jet can merge to a single jet stream (Ahrens and Henson, 2018; Breeden et al., 2021). The tropopause might exhibit an interesting three-dimensional structure during those events. Thus, in Fig. 13, the automatically extracted split and merge events are shown, where split events are encoded with green spheres and merge events with purple spheres. In the images below, a scenario is shown in which jets split or merge depicting how their behavior is influenced by the three-dimensional shape of the tropopause.

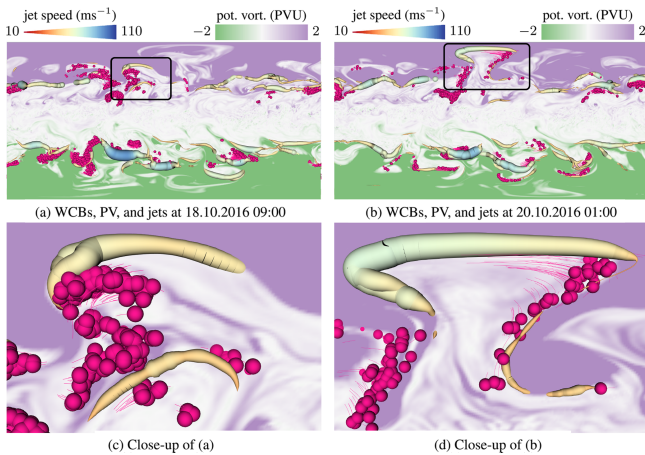


Figure 12. Visualization of jet stream and WCBs together with the potential vorticity at the upper troposphere at 270 hPa. Green values indicate PV smaller than -2 pvu and violet values indicate a PV larger than 2 pvu. White values are close to 0 pvu. On the jet stream, wind speed is mapped to color and tube radius. Panel (a) shows how a WCB pushes against the jet. Panel (b) shows the situation 2 d later. The WCB injected low-PV air masses into the upper troposphere and pushed the jet stream northwards. In panels (c) and (d), close-ups are shown.

Some examples of single-jet and/or double-jet configurations are well known from the North Pacific and North Atlantic, where wave activity can be transferred from one to the other jet (Martius et al., 2010), which can sometimes lead to the merging and/or splitting of jets. In addition to the ocean-wide implication of jet splitting and merging, it is conceivable – yet still not systematically studied – that splitting and merging events are meteorologically “active” regions, for instance, with enhanced probabilities for clear air turbulence (CAT) and thus impact aircraft efficiency and safety (Reiter and Nania, 1964). It will be a rewarding aim to further study these flow regions, not only with respect to CAT but also other meteorological impacts, e.g., stratosphere–troposphere exchange (Akritidis et al., 2016).

6 Conclusions

Jet streams are three-dimensional meteorological flow features that can interact with other atmospheric structures such as warm conveyor belts and the tropopause. We developed an integration-based feature extraction algorithm that locates the explicit jet stream geometry near the tropopause. In contrast to previous local methods (Kern et al., 2017), the predictor–corrector approach allows the wind magnitude ridge lines to be regularized. When the ridge line exhibits high vertical curvature, then regularizing with a smooth vector field helps to produce smoother lines. The high vertical curvature of the ridge line is a product of the low vertical resolution of the hybrid model levels. With an increased model

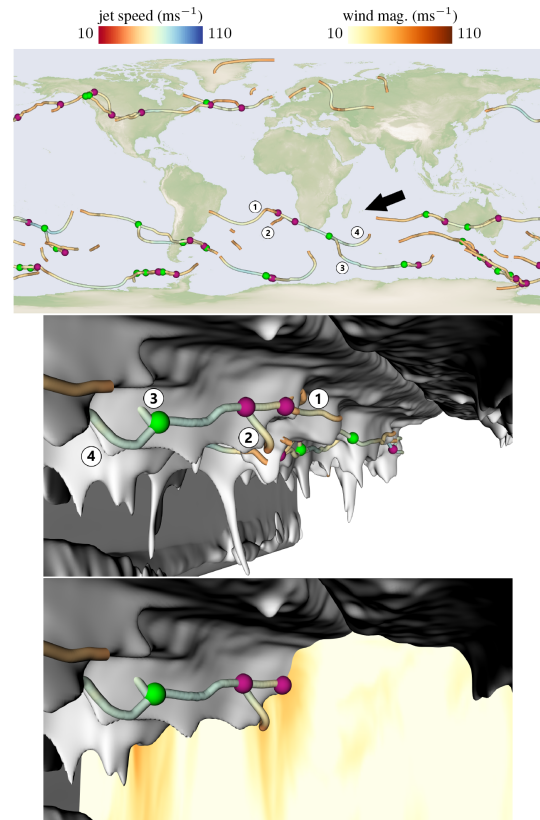


Figure 13. Top: overview visualization of split (green) and merge (purple) events of jet stream core lines at the tropopause. An arrow depicts the camera position of the 3-D views shown from below the tropopause. Middle: a jet (1) moves along a tropopause fold and another jet that passed from below the tropopause fold merges into it (2). The combined jet later splits into two separate branches (3) and (4). Bottom: an orthographic slice color codes the wind magnitude, showing that the jets pass through orange regions (high wind speed). The data here are for 9 September 2016 at 12:00 UTC.

resolution, such regularization will hopefully not be necessary anymore in the future. Apart from this, local feature extractors such as parallel vectors often experience fragmentation independent of the discretization of the domain, resulting in spurious lines that have to be reconnected in a post-process. Predictor–corrector approaches are in the class of integration-based methods, which generally avoid this numerical issue. Given long and coherent jet stream trajectories, we can automatically detect proximities to WCBs and locate split and merge events of jets. To visualize jets along with WCBs and the dynamic tropopause, we developed a visualization system and applied the tool in multiple cases, visualizing the acceleration and displacement of jets near WCBs, and the movement and split and/or merge along tropopause folds. It is known that WCB outflows significantly influence the upper-level waveguide, which is typically identified as a region of enhanced PV gradients on an isentropic surface (Grams et al., 2018; Spreitzer, 2020; Saf-

fin et al., 2021; Grams et al., 2011). However, this perspective does neglect a crucial aspect of the atmospheric flow setting: its three-dimensionality. The distance between the WCB outflow and the waveguide has to be determined. This, however, is no trivial task. It becomes more manageable if the interaction is not only considered in the PV perspective, but instead the WCB outflow trajectories are directly linked to the jet core lines. The feature extraction (WCB, jet core lines, tropopause) developed in this study gives the means to visually inspect co-occurrences of WCB outflows and the jet core lines with respect to their horizontal and vertical position, with the amplitudes (local wind maxima; jet streaks) and their overall geometric structure.

In the future, it would be interesting to extract jet streams automatically for even longer time series. To increase temporal coherence, multiple time steps could be taken into account. Since our extraction traces one jet core line after the other, varying the order in which the seed points are processed influences the jet core-line network, which becomes more noticeable when too little weight was given to the corrector step, i.e., when the lines primarily follow the flow rather than the ridge lines. It would be interesting to investigate how the jets extraction could be made order independent. While the extraction algorithm could be applied to data arising in an operational context, more work is necessary for a successful integration in operational routines, including an increased temporal stability, heuristics for automatic parameter selection, and a requirement analysis with operational forecasters to integrate additional constraints into the feature definition and extraction.

Code and data availability. A C++ implementation of the integration-based jet stream core extraction is available at <https://doi.org/10.5281/zenodo.5567863> (Bösigler et al., 2021b) and on GitHub at <https://github.com/fau-vc/jet-core-extraction> (last access: 23 November 2021). The demo data are published at <https://doi.org/10.5281/zenodo.5567866> (Bösigler et al., 2021a). ERA5 data (<https://doi.org/10.24381/cds.bd0915c6>, Hersbach et al., 2018) are available from the Copernicus Climate Change Service at ECMWF.

Video supplement. A supplemental video shows the extraction results in an animation. The video is made available at <https://doi.org/10.5281/zenodo.5722311> (Bösigler et al., 2021c).

Author contributions. LB implemented the method, conducted the analysis, and wrote the manuscript; MS, MB, HJ, and TG conceived the idea; and MS, MB, and HJ provided the data. All, MS, MB, HJ, and TG supervised the work with regular inputs and contributed to the writing of the manuscript.

Competing interests. The contact author has declared that neither they nor their co-authors have any competing interests.

Disclaimer. Publisher's note: Copernicus Publications remains neutral with regard to jurisdictional claims in published maps and institutional affiliations.

Financial support. This research has been supported by the Schweizerischer Nationalfonds zur Förderung der Wissenschaftlichen Forschung (grant no. PZ00P2_180114) and the European Research Council, H2020 European Research Council (INTEXseas (grant no. 787652)), and the open-access publication funding by the Deutsche Forschungsgemeinschaft and the Friedrich-Alexander-Universität Erlangen-Nürnberg.

Review statement. This paper was edited by Ignacio Pisco and reviewed by Gloria Manney and one anonymous referee.

References

- Ahrens, C. D. and Henson, R.: *Meteorology Today: An Introduction to Weather, Climate and the Environment*, Cengage Learning, Boston, MA, USA, 2021.
- Akritidis, D., Pozzer, A., Zanis, P., Tyrlis, E., Škerlak, B., Sprenger, M., and Lelieveld, J.: On the role of tropopause folds in summertime tropospheric ozone over the eastern Mediterranean and the Middle East, *Atmos. Chem. Phys.*, 16, 14025–14039, <https://doi.org/10.5194/acp-16-14025-2016>, 2016.
- Archer, C. L. and Caldeira, K.: Historical trends in the jet streams, *Geophys. Res. Lett.*, 35, <https://doi.org/10.1029/2008GL033614>, 2008.
- Bader, R., Sprenger, M., Ban, N., Rüdüsühli, S., Schär, C., and Günther, T.: Extraction and Visual Analysis of Potential Vorticity Banners around the Alps, *IEEE T. Vis. Comput. Gr.*, 26, 259–269, <https://doi.org/10.1109/TVCG.2019.2934310>, 2020.
- Banks, D. and Singer, B.: Vortex tubes in turbulent flows: identification, representation, reconstruction, in: *Proceedings Visualization '94*, IEEE Computer Society, Los Alamitos, CA, USA, 21 October 1994, 132–139, <https://doi.org/10.1109/VISUAL.1994.346327>, 1994.
- Barton, N. P. and Ellis, A. W.: Variability in wintertime position and strength of the North Pacific jet stream as represented by re-analysis data, *Int. J. Climatol.*, 29, 851–862, <https://doi.org/10.1002/joc.1750>, 2009.
- Binder, H., Boettcher, M., Joos, H., and Wernli, H.: The Role of Warm Conveyor Belts for the Intensification of Extratropical Cyclones in Northern Hemisphere Winter, *J. Atmos. Sci.*, 73, 3997–4020, <https://doi.org/10.1175/JAS-D-15-0302.1>, 2016.
- Blanchard, N., Pantillon, F., Chaboureaud, J.-P., and Delanoë, J.: Mid-level convection in a warm conveyor belt accelerates the jet stream, *Weather Clim. Dynam.*, 2, 37–53, <https://doi.org/10.5194/wcd-2-37-2021>, 2021.
- Blanco, J. L. and Rai, P. K.: nanoflann: a C++ header-only fork of FLANN, a library for Nearest Neighbor (NN) with KD-

- trees, GitHub [code], available at: <https://github.com/jlblancoc/nanoflann> (last access:23 November 2021), 2014.
- Bösiger, L., Sprenger, M., Boettcher, M., Joos, H., and Günther, T.: Integration-based Extraction and Visualization of Jet Stream Cores – Demo Data, Zenodo [data set], <https://doi.org/10.5281/zenodo.5567866>, 2021a.
- Bösiger, L., Sprenger, M., Boettcher, M., Joos, H., and Günther, T.: Integration-based Extraction and Visualization of Jet Stream Cores – Source Code, Zenodo [code], <https://doi.org/10.5281/zenodo.5567863>, 2021b.
- Bösiger, L., Sprenger, M., Boettcher, M., Joos, H., and Günther, T.: Integration-based Extraction and Visualization of Jet Stream Cores – Supplemental Video, Zenodo, <https://doi.org/10.5281/zenodo.5722311>, 2021c.
- Breeden, M. L., Butler, A. H., Albers, J. R., Sprenger, M., and Langford, A. O.: The spring transition of the North Pacific jet and its relation to deep stratosphere-to-troposphere mass transport over western North America, *Atmos. Chem. Phys.*, 21, 2781–2794, <https://doi.org/10.5194/acp-21-2781-2021>, 2021.
- Cunningham, P. and Keyser, D.: Jet streaks, in: *Encyclopedia of Atmospheric Sciences*, second edn., edited by: North, G. R., Pyle, J., and Zhang, F., Academic Press, Oxford, UK, 359–369, <https://doi.org/10.1016/B978-0-12-382225-3.00187-0>, 2015.
- Dameris, M.: Stratosphere/Troposphere exchange and structure | Tropopause, in: *Encyclopedia of Atmospheric Sciences*, second edn., edited by: North, G. R., Pyle, J., and Zhang, F., Academic Press, Oxford, UK, 269–272, <https://doi.org/10.1016/B978-0-12-382225-3.00418-7>, 2015.
- Danielsen, E. F.: Stratospheric-Tropospheric Exchange Based on Radioactivity, Ozone and Potential Vorticity, *J. Atmos. Sci.*, 25, 502–518, [https://doi.org/10.1175/1520-0469\(1968\)025<0502:STEBOR>2.0.CO;2](https://doi.org/10.1175/1520-0469(1968)025<0502:STEBOR>2.0.CO;2), 1968.
- Davies, H. C.: Weather chains during the 2013/2014 winter and their significance for seasonal prediction, *Nat. Geosci.*, 8, 833–837, 2015.
- Eberly, D.: *Ridges in Image and Data Analysis*, Computational Imaging and Vision, Springer Netherlands, Dordrecht, The Netherlands, <https://doi.org/10.1007/978-94-015-8765-5>, 1996.
- Eckermann, S.: Hybrid σ - p Coordinate Choices for a Global Model, *Mon. Weather Rev.*, 137, 224–245, <https://doi.org/10.1175/2008MWR2537.1>, 2009.
- Eckhardt, S., Stohl, A., Wernli, H., James, P., Forster, C., and Spichtinger, N.: A 15-Year Climatology of Warm Conveyor Belts, *J. Climate*, 17, 218–237, [https://doi.org/10.1175/1520-0442\(2004\)017<0218:AYCOWC>2.0.CO;2](https://doi.org/10.1175/1520-0442(2004)017<0218:AYCOWC>2.0.CO;2), 2004.
- Grams, C. M., Wernli, H., Böttcher, M., Campa, J., Corsmeier, U., Jones, S. C., Keller, J. H., Lenz, C.-J., and Wiegand, L.: The key role of diabatic processes in modifying the upper-tropospheric wave guide: a North Atlantic case-study, *Q. J. Roy. Meteor. Soc.*, 137, 2174–2193, <https://doi.org/10.1002/qj.891>, 2011.
- Grams, C. M., Magnusson, L., and Madonna, E.: An atmospheric dynamics perspective on the amplification and propagation of forecast error in numerical weather prediction models: A case study, *Q. J. Roy. Meteor. Soc.*, 144, 2577–2591, <https://doi.org/10.1002/qj.3353>, 2018.
- Günther, T. and Theisel, H.: The State of the Art in Vortex Extraction, *Comput. Graph. Forum*, 37, 149–173, <https://doi.org/10.1111/cgf.13319>, 2018.
- Harnik, N., Garfinkel, C. I., and Lachmy, O.: The influence of jet stream regime on extreme weather events, in: *Dynamics and Predictability of Large-Scale, High-Impact Weather and Climate Events*, 2, 79–94, <https://doi.org/10.1017/CBO9781107775541.007>, 2016.
- Hersbach, H., Bell, B., Berrisford, P., Biavati, G., Horányi, A., Muñoz Sabater, J., Nicolas, J., Peubey, C., Radu, R., Rozum, I., Schepers, D., Simmons, A., Soci, C., Dee, D., and Thépaut, J.-N.: ERA5 hourly data on pressure levels from 1979 to present, Copernicus Climate Change Service [data set], <https://doi.org/10.24381/cds.bd0915c6>, 2018.
- Hersbach, H., Bell, B., Berrisford, P., Hirahara, S., Horányi, A., Muñoz-Sabater, J., Nicolas, J., Peubey, C., Radu, R., Schepers, D., Simmons, A., Soci, C., Abdalla, S., Abellan, X., Balsamo, G., Bechtold, P., Biavati, G., Bidlot, J., Bonavita, M., De Chiara, G., Dahlgren, P., Dee, D., Diamantakis, M., Dragani, R., Flemming, J., Forbes, R., Fuentes, M., Geer, A., Haimberger, L., Healy, S., Hogan, R. J., Hólm, E., Janisková, M., Keeley, S., Laloyaux, P., Lopez, P., Lupu, C., Radnoti, G., de Rosnay, P., Rozum, I., Vamborg, F., Villaume, S., and Thépaut, J.-N.: The ERA5 global reanalysis, *Q. J. Roy. Meteor. Soc.*, 146, 1999–2049, <https://doi.org/10.1002/qj.3803>, 2020.
- Highwood, E. J., Hoskins, B. J., and Berrisford, P.: Properties of the arctic tropopause, *Q. J. Roy. Meteor. Soc.*, 126, 1515–1532, <https://doi.org/10.1002/qj.49712656515>, 2000.
- Holton, J. R., Haynes, P. H., McIntyre, M. E., Douglass, A. R., Rood, R. B., and Pfister, L.: Stratosphere-troposphere exchange, *Rev. Geophys.*, 33, 403–439, <https://doi.org/10.1029/95RG02097>, 1995.
- Hoskins, B. J., McIntyre, M. E., and Robertson, A. W.: On the use and significance of isentropic potential vorticity maps, *Q. J. Roy. Meteor. Soc.*, 111, 877–946, <https://doi.org/10.1002/qj.49711147002>, 1985.
- Joos, H. and Forbes, R. M.: Impact of different IFS microphysics on a warm conveyor belt and the downstream flow evolution, *Q. J. Roy. Meteor. Soc.*, 142, 2727–2739, <https://doi.org/10.1002/qj.2863>, 2016.
- Kern, M. and Westermann, R.: Clustering Ensembles of 3D Jet-Stream Core Lines, in: *Vision, Modeling and Visualization*, edited by: Schulz, H.-J., Teschner, M., and Wimmer, M., The Eurographics Association, <https://doi.org/10.2312/vmv.20191321>, 2019.
- Kern, M., Hewson, T., Sadlo, F., Westermann, R., and Rautenhaus, M.: Robust Detection and Visualization of Jet-Stream Core Lines in Atmospheric Flow, *IEEE T. Vis. Comput. Gr.*, 24, 893–902, <https://doi.org/10.1109/TVCG.2017.2743989>, 2017.
- Koch, P., Wernli, H., and Davies, H. C.: An event-based jet-stream climatology and typology, *Int. J. Climatol.*, 26, 283–301, <https://doi.org/10.1002/joc.1255>, 2006.
- Kunz, A., Konopka, P., Müller, R., and Pan, L. L.: Dynamical tropopause based on isentropic potential vorticity gradients, *J. Geophys. Res.-Atmos.*, 116, D01110, <https://doi.org/10.1029/2010JD014343>, 2011.
- Lee, S. and Kim, H.-k.: The Dynamical Relationship between Subtropical and Eddy-Driven Jets, *J. Atmos. Sci.*, 60, 1490–1503, [https://doi.org/10.1175/1520-0469\(2003\)060<1490:TDRBSA>2.0.CO;2](https://doi.org/10.1175/1520-0469(2003)060<1490:TDRBSA>2.0.CO;2), 2003.
- Li, S., Jaroszynski, S., Pearse, S., Orf, L., and Clyne, J.: VA-POR: A Visualization Package Tailored to Analyze Simula-

- tion Data in Earth System Science, Atmosphere, 10, 488, <https://doi.org/10.3390/atmos10090488>, 2019.
- Lillo, S. P., Cavallo, S. M., Parsons, D. B., and Riedel, C.: The Role of a Tropopause Polar Vortex in the Generation of the January 2019 Extreme Arctic Outbreak, *J. Atmos. Sci.*, 78, 2801–2821, <https://doi.org/10.1175/JAS-D-20-0285.1>, 2021.
- Limbach, S., Schömer, E., and Wernli, H.: Detection, tracking and event localization of jet stream features in 4-D atmospheric data, *Geosci. Model Dev.*, 5, 457–470, <https://doi.org/10.5194/gmd-5-457-2012>, 2012.
- Ljung, P. and Ynnerman, A.: Extraction of intersection curves from iso-surfaces on co-located 3d grids, in: The Annual SIGRAD Conference. Special Theme-Real-Time Simulations, Conference Proceedings from SIGRAD2003, Umeå, Sweden, 20–21 November 2003, 23–28, <https://ep.liu.se/ecp/010/006/ecp01006.pdf> (last access: 23 November 2022), 2003.
- Madonna, E., Wernli, H., Joos, H., and Martius, O.: Warm Conveyor Belts in the ERA-Interim Dataset (1979–2010). Part I: Climatology and Potential Vorticity Evolution, *J. Climate*, 27, 3–26, <https://doi.org/10.1175/JCLI-D-12-00720.1>, 2014.
- Maher, P., Kelleher, M., Sansom, P., and Methven, J.: Is the subtropical jet shifting poleward?, *Clim. Dynam.*, 54, 1741–1759, <https://doi.org/10.1007/s00382-019-05084-6>, 2019.
- Manney, G. L. and Hegglin, M. I.: Seasonal and Regional Variations of Long-Term Changes in Upper-Tropospheric Jets from Reanalyses, *J. Climate*, 31, 423–448, <https://doi.org/10.1175/JCLI-D-17-0303.1>, 2018.
- Manney, G. L., Hegglin, M. I., Daffer, W. H., Santee, M. L., Ray, E. A., Pawson, S., Schwartz, M. J., Boone, C. D., Froidevaux, L., Livesey, N. J., Read, W. G., and Walker, K. A.: Jet characterization in the upper troposphere/lower stratosphere (UTLS): applications to climatology and transport studies, *Atmos. Chem. Phys.*, 11, 6115–6137, <https://doi.org/10.5194/acp-11-6115-2011>, 2011.
- Manney, G. L., Hegglin, M. I., Daffer, W. H., Schwartz, M. J., Santee, M. L., and Pawson, S.: Climatology of Upper Tropospheric – Lower Stratospheric (UTLS) Jets and Tropopauses in MERRA, *J. Climate*, 27, 3248–3271, <https://doi.org/10.1175/JCLI-D-13-00243.1>, 2014.
- Manney, G. L., Hegglin, M. I., and Lawrence, Z. D.: Seasonal and regional signatures of ENSO in upper tropospheric jet characteristics from reanalyses, *J. Climate*, 34, 9181–9200, <https://doi.org/10.1175/JCLI-D-20-0947.1>, 2021.
- Martius, O.: A Lagrangian Analysis of the Northern Hemisphere Subtropical Jet, *J. Atmos. Sci.*, 71, 2354–2369, <https://doi.org/10.1175/JAS-D-13-0329.1>, 2014.
- Martius, O., Schwierz, C., and Davies, H. C.: Tropopause-Level Waveguides, *J. Atmos. Sci.*, 67, 866–879, <https://doi.org/10.1175/2009JAS2995.1>, 2010.
- Nielsen-Gammon, J. W.: A Visualization of the Global Dynamic Tropopause, *B. Am. Meteorol. Soc.*, 82, 1151–1168, [https://doi.org/10.1175/1520-0477\(2001\)082<1151:AVOTGD>2.3.CO;2](https://doi.org/10.1175/1520-0477(2001)082<1151:AVOTGD>2.3.CO;2), 2001.
- Oertel, A., Boettcher, M., Joos, H., Sprenger, M., Konow, H., Hagen, M., and Wernli, H.: Convective activity in an extratropical cyclone and its warm conveyor belt – a case-study combining observations and a convection-permitting model simulation, *Q. J. Roy. Meteor. Soc.*, 145, 1406–1426, <https://doi.org/10.1002/qj.3500>, 2019.
- Oertel, A., Boettcher, M., Joos, H., Sprenger, M., and Wernli, H.: Potential vorticity structure of embedded convection in a warm conveyor belt and its relevance for large-scale dynamics, *Weather Clim. Dynam.*, 1, 127–153, <https://doi.org/10.5194/wcd-1-127-2020>, 2020.
- Peikert, R. and Roth, M.: The “Parallel Vectors” operator – a vector field visualization primitive, in: Proceedings Visualization '99 (Cat. No.99CB37067), San Francisco, CA, USA, 24–29 October 1999, 263–532, <https://doi.org/10.1109/VISUAL.1999.809896>, 1999.
- Pena-Ortiz, C., Gallego, D., Ribera, P., Ordóñez, P., and Alvarez-Castro, M. D. C.: Observed trends in the global jet stream characteristics during the second half of the 20th century, *J. Geophys. Res.-Atmos.*, 118, 2702–2713, <https://doi.org/10.1002/jgrd.50305>, 2013.
- Rautenhaus, M., Grams, C. M., Schäfler, A., and Westermann, R.: Three-dimensional visualization of ensemble weather forecasts – Part 2: Forecasting warm conveyor belt situations for aircraft-based field campaigns, *Geosci. Model Dev.*, 8, 2355–2377, <https://doi.org/10.5194/gmd-8-2355-2015>, 2015a.
- Rautenhaus, M., Kern, M., Schäfler, A., and Westermann, R.: Three-dimensional visualization of ensemble weather forecasts – Part 1: The visualization tool Met.3D (version 1.0), *Geosci. Model Dev.*, 8, 2329–2353, <https://doi.org/10.5194/gmd-8-2329-2015>, 2015b.
- Rautenhaus, M., Böttinger, M., Siemen, S., Hoffman, R., Kirby, R. M., Mirzargar, M., Röber, N., and Westermann, R.: Visualization in Meteorology – A Survey of Techniques and Tools for Data Analysis Tasks, *IEEE T. Vis. Comput. Gr.*, 24, 3268–3296, <https://doi.org/10.1109/TVCG.2017.2779501>, 2018.
- Raveh-Rubin, S.: Dry Intrusions: Lagrangian Climatology and Dynamical Impact on the Planetary Boundary Layer, *J. Climate*, 30, 6661–6682, <https://doi.org/10.1175/JCLI-D-16-0782.1>, 2017.
- Reiter, E. R. and Nania, A.: Jet-stream structure and clear-air turbulence (CAT), *J. Appl. Meteorol. Clim.*, 3, 247–260, 1964.
- Rodwell, M., Forbes, R., and Wernli, H.: Why warm conveyor belts matter in NWP, ECMWF newsletter, 21–28, <https://doi.org/10.21957/mr20vg>, 2018.
- Rodwell, M. J., Magnusson, L., Bauer, P., Bechtold, P., Bonavita, M., Cardinali, C., Diamantakis, M., Earnshaw, P., García-Méndez, A., Isaksen, I., Källén, E., Klocke, D., Lopez, P., McNally, T., Persson, A., Prates, F., and Wedi, N.: Characteristics of occasional poor medium-range weather forecasts for Europe, *B. Am. Meteorol. Soc.*, 94, 1393–1405, 2013.
- Saffin, L., Methven, J., Bland, J., Harvey, B., and Sanchez, C.: Circulation conservation in the outflow of warm conveyor belts and consequences for Rossby wave evolution, *Q. J. Roy. Meteor. Soc.*, 147, 3587–3610, <https://doi.org/10.1002/qj.4143>, 2021.
- Schiemann, R., Lüthi, D., and Schär, C.: Seasonality and Interannual Variability of the Westerly Jet in the Tibetan Plateau Region, *J. Climate*, 22, 2940–2957, <https://doi.org/10.1175/2008JCLI2625.1>, 2009.
- Schoeberl, M. R.: Extratropical stratosphere-troposphere mass exchange, *J. Geophys. Res.-Atmos.*, 109, D13303, <https://doi.org/10.1029/2004JD004525>, 2004.
- Schroeder, W. J., Martin, K., and Lorenzen, W. E.: The visualization toolkit, 4. edn., Kitware, Clifton Park, N.Y., 528 pp., ISBN 978 1930934191, 2006.
- Schultz, D. M., Bosart, L. F., Colle, B. A., Davies, H. C., Dearden, C., Keyser, D., Martius, O., Roebber, P. J., Steenburgh, W. J.,

- Volkert, H., and Winters, A. C.: Extratropical Cyclones: A Century of Research on Meteorology's Centerpiece, *Meteor. Mon.*, 59, 16.1–16.56, <https://doi.org/10.1175/AMSMONOGRAPHS-D-18-0015.1>, 2019.
- Schäfler, A., Craig, G., Wernli, H., Arbogast, P., Doyle, J. D., McTaggart-Cowan, R., Methven, J., Rivière, G., Ament, F., Boettcher, M., Bramberger, M., Cazenave, Q., Cotton, R., Crewell, S., Delanoë, J., Dörnbrack, A., Ehrlich, A., Ewald, F., Fix, A., Grams, C. M., Gray, S. L., Grob, H., Groß, S., Hagen, M., Harvey, B., Hirsch, L., Jacob, M., Kölling, T., Konow, H., Lemmerz, C., Lux, O., Magnusson, L., Mayer, B., Mech, M., Moore, R., Pelon, J., Quinting, J., Rahm, S., Rapp, M., Rautenhaus, M., Reitebuch, O., Reynolds, C. A., Sodemann, H., Spengler, T., Vaughan, G., Wendisch, M., Wirth, M., Witschas, B., Wolf, K., and Zinner, T.: The North Atlantic Waveguide and Downstream Impact Experiment, *B. Am. Meteorol. Soc.*, 99, 1607–1637, <https://doi.org/10.1175/BAMS-D-17-0003.1>, 2018.
- Shapiro, M. A.: Turbulent Mixing within Tropopause Folds as a Mechanism for the Exchange of Chemical Constituents between the Stratosphere and Troposphere, *J. Atmos. Sci.*, 37, 994–1004, [https://doi.org/10.1175/1520-0469\(1980\)037<0994:TMWTF>2.0.CO;2](https://doi.org/10.1175/1520-0469(1980)037<0994:TMWTF>2.0.CO;2), 1980.
- Shapiro, M. A. and Keyser, D.: Fronts, jet streams and the tropopause, in: *Extratropical cyclones*, American Meteorological Society, Boston, MA, USA, 167–191, https://doi.org/10.1007/978-1-944970-33-8_10, 1990.
- Škerlak, B., Sprenger, M., Pfahl, S., Tyrlis, E., and Wernli, H.: Tropopause folds in ERA-Interim: Global climatology and relation to extreme weather events, *J. Geophys. Res.-Atmos.*, 120, 4860–4877, <https://doi.org/10.1002/2014JD022787>, 2015.
- Spensberger, C. and Spengler, T.: Feature-Based Jet Variability in the Upper Troposphere, *J. Climate*, 33, 6849–6871, <https://doi.org/10.1175/JCLI-D-19-0715.1>, 2020.
- Spensberger, C., Spengler, T., and Li, C.: Upper-tropospheric jet axis detection and application to the boreal winter 2013/14, *Mon. Weather Rev.*, 145, 2363–2374, 2017.
- Spreitzer, E. J.: Diabatic processes in mid-latitude weather systems – a study with the ECMWF model, Ph.D. thesis, ETH Zurich, <https://doi.org/10.3929/ethz-b-000438728>, 2020.
- Sprenger, M., Croci Maspoli, M., and Wernli, H.: Tropopause folds and cross-tropopause exchange: A global investigation based upon ECMWF analyses for the time period March 2000 to February 2001, *J. Geophys. Res.-Atmos.*, 108, 8518, <https://doi.org/10.1029/2002JD002587>, 2003.
- Steinfeld, D., Boettcher, M., Forbes, R., and Pfahl, S.: The sensitivity of atmospheric blocking to upstream latent heating – numerical experiments, *Weather Clim. Dynam.*, 1, 405–426, <https://doi.org/10.5194/wcd-1-405-2020>, 2020.
- Stohl, A., Bonasoni, P., Cristofanelli, P., Collins, W., Feichter, J., Frank, A., Forster, C., Gerasopoulos, E., Gäggeler, H., James, P., Kentarchos, T., Kromp-Kolb, H., Krüger, B., Land, C., Meloan, J., Papayannis, A., Priller, A., Seibert, P., Sprenger, M., Roelofs, G. J., Scheel, H. E., Schnabel, C., Siegmund, P., Tobler, L., Trickl, T., Wernli, H., Wirth, V., Zanis, P., and Zerefos, C.: Stratosphere-troposphere exchange: A review, and what we have learned from STACCATO, *J. Geophys. Res.-Atmos.*, 108, 8516, <https://doi.org/10.1029/2002JD002490>, 2003.
- Van Gelder, A. and Pang, A.: Using PVsolve to Analyze and Locate Positions of Parallel Vectors, *IEEE T. Vis. Comput. Gr.*, 15, 682–695, <https://doi.org/10.1109/TVCG.2009.11>, 2009.
- Weinkauff, T., Theisel, H., Van Gelder, A., and Pang, A.: Stable Feature Flow Fields, *IEEE T. Vis. Comput. Gr.*, 17, 770–780, <https://doi.org/10.1109/TVCG.2010.93>, 2011.
- Wernli, H.: A lagrangian-based analysis of extratropical cyclones. II: A detailed case-study, *Q. J. Roy. Meteor. Soc.*, 123, 1677–1706, <https://doi.org/10.1002/qj.49712354211>, 1997.
- Wernli, H. and Schwierz, C.: Surface Cyclones in the ERA-40 Dataset (1958–2001). Part I: Novel Identification Method and Global Climatology, *J. Atmos. Sci.*, 63, 2486–2507, <https://doi.org/10.1175/JAS3766.1>, 2006.
- Winters, A. C., Keyser, D., Bosart, L. F., and Martin, J. E.: Composite Synoptic-Scale Environments Conducive to North American Polar? Subtropical Jet Superposition Events, *Mon. Weather Rev.*, 148, 1987–2008, <https://doi.org/10.1175/MWR-D-19-0353.1>, 2020.
- Witschi, R. and Günther, T.: Implicit Ray Casting of the Parallel Vectors Operator, in: *IEEE Visualization – Short Papers*, 25–30 October 2020, Salt Lake City, UT, USA, 31–35, <https://doi.org/10.1109/VIS47514.2020.00013>, 2020.
- WMO: International meteorological vocabulary, second edn., Secretariat Of The World Meteorological Organization, Geneva, Switzerland, ISBN 9789263021823, 1992.